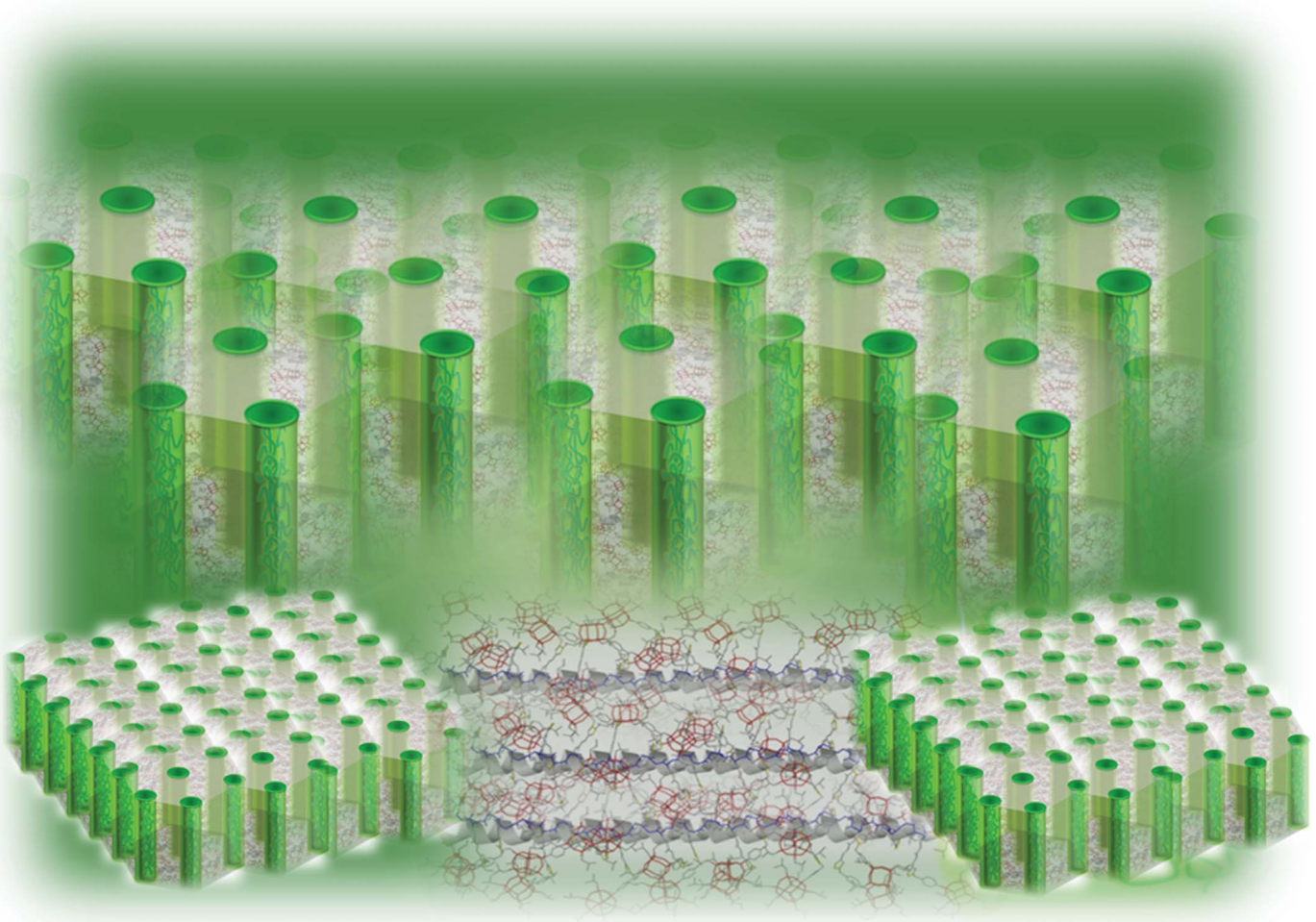

The "Supramolecular Polymer Chemistry and Physics" lab established and headed by Dr. Shiao-Wei Kuo at National Sun Yat-Sen University, Taiwan, has an interdisciplinary focus on non-covalent bond interaction, self-assembly supramolecular nanostructures and nanocomposites.

Title: Hierarchical self-assembly structures of POSS-containing polypeptide block copolymers synthesized using a combination of ATRP, ROP and click chemistry

Hierarchical self-assembly structures of POSS-containing polypeptide block copolymers including cylindrical structures as a result of microphase separation of the diblock copolymer, α-helical conformations of polypeptide segments, and aggregation of the POSS moieties.

As featured in:

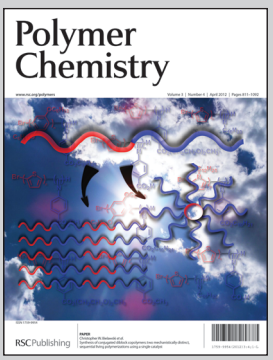

See Y.-C. Lin *et al.*, *Polym. Chem.*, 2012, **3**, 882.

RSC Publishing

www.rsc.org/polymers

Registered Charity Number 207890

Polymer Chemistry

Dynamic Article Links

Cite this: *Polym. Chem.*, 2012, **3**, 882

www.rsc.org/polymers

PAPER

Hierarchical self-assembly structures of POSS-containing polypeptide block copolymers synthesized using a combination of ATRP, ROP and click chemistry

Yung-Chih Lin and Shiao-Wei Kuo*

Received 5th December 2011, Accepted 9th January 2012
DOI: 10.1039/c2py00574c

In this study, we used a combination of atom transfer radical polymerization, ring opening polymerization, and click chemistry to synthesize new organic/inorganic macromolecular self-assembling building blocks of polystyrene-*b*-poly(γ-propargyl-L-glutamate-*g*-polyhedral oligomeric silsesquioxane) [PS-*b*-(PPLG-*g*-POSS)]. The incorporation of the PS and POSS units enhanced the α-helical conformation in the solid state, as determined using Fourier transform infrared (FTIR) spectroscopy and wide-angle X-ray diffraction (WAXD). Hierarchical self-assembly of the PS-*b*-(PPLG-*g*-POSS) diblock copolymers, which we characterized using WAXD, small-angle X-ray scattering, and transmission electron microscopy, led to the formation of cylindrical structures as a result of microphase separation of the diblock copolymer; the hexagonal cylinder packing nanostructure featured α-helical conformations of polypeptide segments, which were oriented perpendicular to the direction of the cylinder column from diblock copolymers; aggregation of the POSS moieties induced the packing into hexagonal lattice structures. The attachment of POSS units onto the side chains of PPLG stabilized the α-helical secondary structures at elevated temperature, relative to those of pure PPLG and PS-*b*-PPLG, as determined through temperature-dependent FTIR spectroscopic analyses.

Introduction

Self-organizing materials allow the development of relatively simple "bottom-up" methods for the low-cost fabrication of large-area periodic nanostructures through the self-assembly of, for example, diblock copolymers.[1–3] Most of the diblock copolymers that have been used for nanofabrication including polystyrene-*b*-poly(4-vinyl pyridine) (PS-*b*-P4VP),[4–6] polystyrene-*b*-polyvinylphenol (PS-*b*-PVPh),[7–9] polystyrene-*b*-polylactide (PS-*b*-PLA),[10–12] and polystyrene-*b*-poly(ethylene oxide) (PS-*b*-PEO)[13–15] have been organic/organic block copolymers. In addition, some organic/inorganic hybrid block copolymers including polystyrene-*b*-polydimethylsiloxane (PS-*b*-PDMS)[16,17] and polystyrene-*b*-polyferrocenylsilane (PS-*b*-PFS)[18] have also received attention for use in integrated circuit processing.

Polyhedral oligomeric silsesquioxane (POSS) derivatives are inorganic block segments that comprise a family of molecularly precise and near-isotropic molecules. POSS structures have diameters ranging from 1 to 3 nm depending on the number of Si atoms in the central cage and the nature of the peripheral substituent groups.[19–26] A cubic T_8 silsesquioxane unit possesses a cubic inorganic Si_8O_{12} core surrounded by eight tunable substituent groups. POSS has been recognized as a well-defined building block for preparing nanostructured materials.[27–32] Pyun and Matyjaszewski used atom transfer radical polymerization (ATRP) to synthesize methacrylo-POSS block copolymers from a cyclopentyl-substituted POSS monomer and *n*-butyl acrylate.[33,34] Lee and coworkers[35–37] used hydrosilylation to prepare an organic/inorganic triblock copolymer of styrene-*b*-butadiene-*b*-styrene (SBS) containing grafted POSS units. Their POSS derivative was designed to contain a single silane functional group for grafting onto 1,2-butadiene units in the polybutadiene (PB) soft block. Because these POSS moieties were dispersed on the molecular scale, the SBS copolymer gradually lost its long-range ordering upon increasing the POSS content; small-angle X-ray scattering (SAXS) analysis revealed that the scattering of the cylindrical structure became diffuse with the lamellar structure and transformed into a perforated layer morphology. Hirai and coworkers[38,39] prepared two kinds of POSS-containing block copolymers, PMMA-*b*-PMAPOSS and PS-*b*-PMAPOSS, through anionic living polymerization and found that they self-assembled into various structures, including spherical, cylindrical, and lamellar morphologies.[39] When applied in lithography processes, these diblock copolymers, with narrow polydispersity, resulted in well-defined morphologies.[40] Those studies, however, were focused only on POSS-containing

Department of Materials and Optoelectronic Science, Center for Nanoscience and Nanotechnology, National Sun Yat-Sen University, Kaohsiung, 804, Taiwan. E-mail: kuosw@faculty.nsysu.edu.tw

coil-based polymer chains; the motivation of our present study was to investigate the self-assembly of POSS-containing rigid-rod polypeptide chains.

The rod segment of the block copolymer developed in this study was the polypeptide poly(L-glutamate). This polypeptide forms hierarchically ordered structures, with α-helical rod-like secondary structures (stabilized through intramolecular hydrogen bonds) and β-sheet secondary structures (stabilized through intermolecular hydrogen bonds).[41] For several decades, most methods for synthesizing poly(peptide-*b*-nonpeptide) (rod/coil) block copolymers, with potential applications in tissue engineering and drug delivery, have followed Nature's strategies for producing these supramolecular bioactive assemblies.[42–50] The nonpeptide blocks [*e.g.*, PS,[47] PEO,[51] PDMS,[52] poly(ε-caprolactone),[53] poly(*N*-isopropylacrylamide),[54] PB,[55] polyisoprene,[56] poly(2-ethyl-2-oxazoline),[57] and polyfluorene[58]] have often been used as macroinitiators. Using Fourier transform infrared (FTIR) spectroscopy, Klok *et al.* found that poly(styrene-*b*-γ-benzyl-L-glutamate) (PS-*b*-PBLG) copolymers featured significantly stabilized α-helical secondary structures relative to those of the corresponding PBLG oligomers.[47]

In this study, we used ATRP, ring opening polymerization (ROP), and click chemistry to combine all of the advantageous features arising from self-assembly microphase separation of diblock copolymers, POSS nanoparticles, and helical polypeptides into the same polymer chain. First, we synthesized a PS derivative through ATRP using (1-bromoethyl)benzene as an initiator and then treated it with NaN_3 to obtain the azide-terminated polystyrene, which we reduced (PPh_3 in THF/water) to the primary amine-terminated polystyrene macroinitiator (PS–NH_2). Next, we prepared polystyrene-*b*-poly(γ-propargyl-L-glutamate) (PS-*b*-PPLG) copolymers through ROP of the monomer γ-propargyl-L-glutamate *N*-carboxyanhydride (PLG-NCA), using PS–NH_2 as the macroinitiator. Finally, we used click reactions to synthesize PS-*b*-(PPLG-*g*-POSS) copolymers from an azido-functionalized POSS derivative (N_3–POSS) and PS-*b*-PPLG. Scheme 1 summarizes all these reactions. We used FTIR spectroscopy, wide-angle X-ray diffraction (WAXD), SAXS, and transmission electron microscopy (TEM) to analyze the hierarchical self-assembled and secondary structures of PS-*b*-PPLG and PS-*b*-(PPLG-*g*-POSS).

Experimental

Materials

Styrene (Aldrich) was vacuum-distilled over CaH_2 and stored under N_2 at −10 °C. Isobutyltrisilanol-POSS was obtained from Hybrid Plastics. Propargyl alcohol and L-glutamic acid were purchased from Tokyo Kasei Kogyo. Copper(I) bromide (CuBr) was purified by washing with glacial AcOH overnight, followed by washing with absolute EtOH and diethyl ether and then drying under vacuum. *N*,*N*-Dimethylformamide (DMF), NaN_3, triethylamine (TEA), 1-phenylethyl bromide, trichloro[4-(chloromethyl)phenyl]silane, PPh_3, and *N*,*N*,*N*′,*N*″,*N*″-pentamethyldiethylenetriamine (PMDETA, 99%) were purchased from Aldrich. All solvents were distilled prior to use. Mono(benzyl

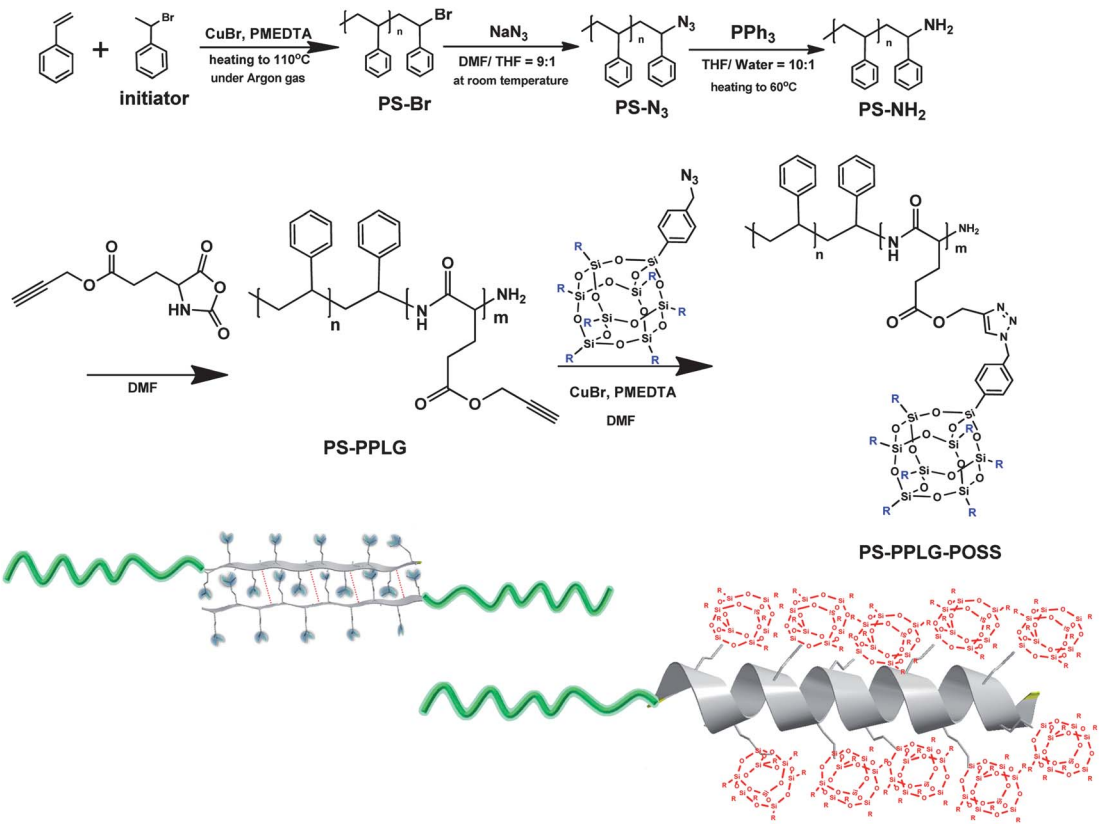

Scheme 1 Synthesis of PS-*b*-PPLG and PS-*b*-(PPLG-*g*-POSS) diblock copolymers.

azide) POSS (N_3–POSS) and γ-propargyl-L-glutamate were prepared according to previous literature procedures.[59–62]

Controlled radical polymerization of PS using ATRP (PS–Br)

CuBr (96 mg, 0.66 mmol) (green powder) was placed in the reactor and degassed under vacuum; dry styrene (20.48 g, 0.20 mol) and (1-bromoethyl)benzene (122 mg, 0.66 mmol) as monomer and initiator, respectively, were added *via* syringe. The mixture was subjected to at least two freeze/pump/thaw cycles. Next, the ligand PMDETA (106 mg, 0.66 mmol) was added *via* syringe under an Ar gas atmosphere and then the system was once again subjected to a freeze/pump/thaw cycle. The reactor was placed in an oil bath and heated at 110 °C for 2 h. When the reaction was complete, the mixture was diluted with THF and passed through a neutral alumina column to remove the catalyst. The solvent was removed from the polymer solution using a rotary evaporator. The polymer was precipitated with MeOH and collected by filtration. The PS powder was dried under vacuum (13.48 g, 80%). ^{1}H NMR ($CDCl_3$, δ): 7.23–6.40 (phenyl protons of PS), 4.60–4.30 [C*H*(Ph)–Br, end group of PS], 2.50–1.20 [CH_2C*H*(Ph), repeating unit of PS].

Preparation of azide-terminated polystyrene (PS–N_3)

The bromine-terminated polystyrene (15.0 g, 2.42 mmol) and NaN_3 (1.57 g, 20.42 mmol) were placed in the reactor and degassed under vacuum. A mixture of dry DMF and THF (9 : 1) was added to the reactor *via* syringe. The reaction mixture was stirred overnight at room temperature; the polymer was isolated through precipitation in water and MeOH to remove the NaBr and unreacted NaN_3. The polymer powder was dried under vacuum and stored in a freezer (13.48 g, 90%). ^{1}H NMR ($CDCl_3$, δ): 7.23–6.40 (phenyl protons of PS), 3.9 [C*H*(Ph)–N_3, end group of PS], 2.50–1.20 [CH_2C*H*(Ph), repeating unit of PS].

Preparation of amine-terminated polystyrene macroinitiator (PS–NH_2)

A solution of the azide-terminated polystyrene (5 g, 0.81 mmol) and PPh_3 (1.06 g, 4.05 mmol; 5 equiv.) in THF and water (10 : 1) was heated overnight at 60 °C. Rotary evaporation of the solvent gave a residue, which was purified through precipitation in MeOH. The amine-terminated PS powder was dried under vacuum (2.23 g, 45%). ^{1}H NMR ($CDCl_3$, δ): 7.23–6.40 (phenyl protons of PS), 3.49 [C*H*(Ph)–NH_2, end group of PS], 2.50–1.20 [CH_2C*H*(Ph), repeating unit of PS].

Controlled ROP of *N*-carboxyanhydride (PS-*b*-PPLG)

The γ-propargyl-L-glutamate *N*-carboxyanhydride (PLG–NCA) (0.50 g, 2.37 mmol) was frozen using liquid N_2 under vacuum conditions. DMF was added *via* syringe and then the solution was warmed to 0 °C. N_2 gas then filled the reactor. The amino-terminated macroinitiator PS–NH_2 (1.47 g, 0.24 mmol) was added and then the mixture was stirred for 48 h at a lower temperature. After evaporation of the solvent under vacuum, the solid residue was dissolved in DMF and precipitated with cold diethyl ether. The pure polymer was collected by filtration and then the solid was dried under vacuum at room temperature.

Synthesis of POSS-containing polypeptide block copolymers [PS-*b*-(PPLG-*g*-POSS)] *via* click chemistry

N_3–POSS (2.27 g, 2.40 mmol), PS-*b*-PPLG (0.20 g, 1.20 mmol), and CuBr (0.17 g, 1.18 mmol) were dissolved in DMF (25 mL) in a flask equipped with a magnetic stirrer bar. After the freeze/thaw/pump cycle, PMDETA (24.6 μL, 1.18 mmol) was added. The reaction mixture was then carefully degassed through three freeze/thaw/pump cycles, placed in an oil bath thermostatted at 60 °C, and stirred for 24 h. After evaporating all of the solvent under reduced pressure, the residue was dissolved in THF and passed through a neutral alumina column to remove the copper catalyst. The THF was evaporated and the product was precipitated using MeOH. The resulting polymer was filtered off and dried under vacuum at room temperature, yielding PS-*b*-(PPLG-*g*-POSS) as a white powder.

Characterization

^{1}H NMR spectra were recorded at room temperature using a Bruker AM 500 (500 MHz) spectrometer, with the residual proton resonance of the deuterated solvent acting as the internal standard. Molecular weights and molecular weight distributions were determined through gel permeation chromatography (GPC) using a Waters 510 high-performance liquid chromatograph equipped with a 410 differential refractometer and three Ultrastyragel columns (100, 500, and 10^3 Å) connected in series, with DMF at 80 °C as the eluent (flow rate: 0.4 mL min^{-1}). The narrow molecular weight distribution polystyrene as standard was used for calibration. Differential scanning calorimetry (DSC) was performed using a TA-Q20 instrument operated at a scan rate of 10 °C min^{-1} over a temperature range of −90 to 200 °C under a N_2 atmosphere. FTIR spectra of the polymer films were recorded using the conventional KBr disk method. The films used in this study were sufficiently thin to obey the Beer–Lambert law. FTIR spectra were recorded using a Bruker Tensor 27 FTIR spectrophotometer; 32 scans were collected at a spectral resolution of 1 cm^{-1}. Mass spectra were obtained using a Bruker Daltonics Autoflex III MALDI-TOF mass spectrometer and the following voltage parameters: ion source 1, 19.06 kV; ion source 2, 16.61 kV; lens, 8.78 kV; reflector 1, 21.08 kV; reflector 2, 9.73 kV. X-Ray diffraction (XRD) data were collected using the wiggler beamline BL17A1 of the National Synchrotron Radiation Research Center (NSRRC), Taiwan. A triangular bent Si (111) single crystal was employed to obtain a monochromated beam with a wavelength (λ) of 1.33001 Å. The XRD patterns were collected using an imaging plate (IP; Fuji BAS III; area = 20 × 40 cm^2) curved with a radius equivalent to the sample-to-detector distance (280 mm). The two-dimensional (2D) XRD patterns observed for the sample (typical diameter: 10 mm; thickness: 1 mm) were circularly averaged to obtain a one-dimensional (1D) diffraction profile $I(Q)$. The value of Q was calibrated using standard samples of silver behenate and Si powder (NBS 640b). SAXS experiments were performed using the SWAXS instrument at the BL17B3 beamline of the NSRRC, Taiwan; the X-ray beam had a diameter of 0.5 mm and a wavelength (λ) of 1.24 Å. The blend samples (thickness: 1 mm) were sealed between two thin Kapton windows (thickness: 80 μm) and analyzed at room temperature. TEM images were recorded using a JEOL-2100

transmission electron microscope operated at an accelerating voltage of 200 kV. Ultrathin sections of the TEM samples (thickness: *ca.* 70 nm) were prepared using a Leica Ultracut UCT microtome equipped with a diamond knife.

Results and discussion

ATRP of polystyrene and ROP of *N*-carboxyanhydride (PS-*b*-PPLG)

The signals in the MALDI-TOF mass spectrum of PS–NH_2 (Fig. 1) are separated by 104 Da, the molecular weight of a styrene unit and Table 1 lists the molecular weight of PS. Fig. 2 displays room-temperature FTIR spectra of the bromo-, azido- and amino-terminated PS derivatives and the corresponding block copolymer PS-*b*-$PPLG_{10}$. Substitution of the bromine atom with the azide group led to the appearance of a stretching vibration band for the azido group at 2096 cm^{-1} (Fig. 2(b)). The spectrum of amino-terminated PS revealed that the signal for the azido group had totally disappeared, with the appearance of new absorbances at 3413 and 3294 cm^{-1} representing the primary amino groups (Fig. 2(c)). After ROP of the γ-propargyl-L-glutamate NCA monomer using PS–NH_2 as the macroinitiator, the FTIR spectrum (Fig. 2(d)) featured new absorbances at 1653, 1627, and 1543 cm^{-1}, representing the amide bonds in the polymer backbone, with the acetylene C≡C stretching vibration at 2130 cm^{-1} remaining for PS-*b*-PPLG. Fig. 3(a) presents the ^{1}H NMR spectrum of the PS–NH_2 macroinitiator in $CDCl_3$. The signals at 6.40–7.23 and 1.20–2.50 ppm correspond to the aromatic (protons 4) and aliphatic CH_2CH(Ph) (protons 2 and 3) protons, respectively. We assigned the singlet at 3.49 ppm to the methine proton adjacent to the terminal polystyrene amino group. Fig. 3(b) displays the ^{1}H NMR spectrum of PS-*b*-$PPLG_{10}$ in $CDCl_3$ and 15 wt% TFA. The signal for the proton on the nitrogen atom of PPLG appeared as a singlet at 7.95 ppm; the singlets at 2.50 and 4.78 ppm corresponded to the *H*C≡C–C and C≡C–CH_2 protons, respectively. The signals of the PS block appeared at 1.30–1.98 [CH_2CH(Ph)], 4.42 [C*H*(Ph)NH], and 6.38–7.23 (phenyl protons of PS) ppm. We determined the molar masses of the PS-*b*-PPLG copolymers from their ^{1}H NMR spectra using the equation:

$$M_{n,\text{PS-}b\text{-PPLG}} = \frac{5I_a M_{\text{PLG}}}{I_4} + M_{\text{PS-amine}}$$

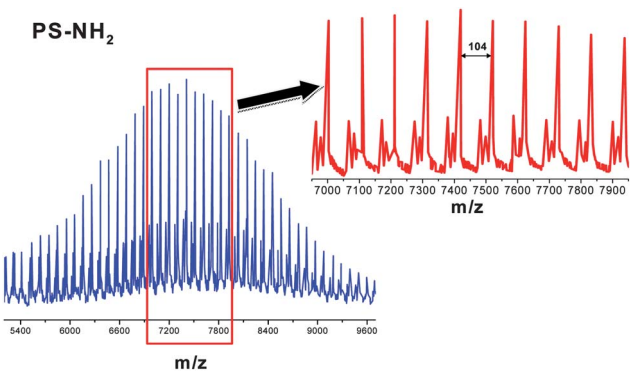

Fig. 1 MALDI-TOF mass spectrum of PS–NH_2.

Table 1 Characterizations of PS and PS-*b*-PPLG used in this study

Polymer	M_n[a]	M_n[b]	PDI[b]
PS–NH_2	6240	6920	1.07
PS-*b*-$PPLG_{10}$	7900	11 300	1.09
PS-*b*-$PPLG_{20}$	9600	15 700	1.14

[a] Determined from ^{1}H NMR spectra. [b] Determined from GPC analysis.

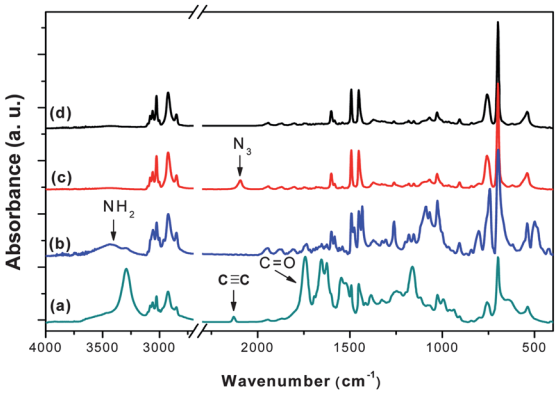

Fig. 2 FTIR spectra of (a) PS–Br, (b) PS–N_3, (c) PS–NH_2 and (d) PS-*b*-$PPLG_{10}$.

where I_b and I_4 are the intensities of the signals of the acetylene protons *a* on the side chains of PS-*b*-PPLG and of the phenyl protons 4 of the PS–amine macroinitiator, respectively, and $M_{\text{PS–amine}}$ is the molar mass of the PS–NH_2 macroinitiator. Fig. 4 displays GPC traces of the PS–NH_2 macroinitiator, PS-*b*-$PPLG_{10}$ and PS-*b*-$PPLG_{20}$; each reveals a narrow molecular weight distribution (<1.15). Block copolymers prepared from the PS macroinitiator resulted in products with narrow polydispersity and high symmetry, with monomodal GPC traces. The absence of the PS–NH_2 macroinitiator peak supports the formation of the PS-*b*-PPLG diblock copolymers, with the peak maxima of these spectra clearly shifting to higher molecular weight upon increasing the ratio of the PLG NCA monomer to PS–NH_2 macroinitiator. Table 1 lists the

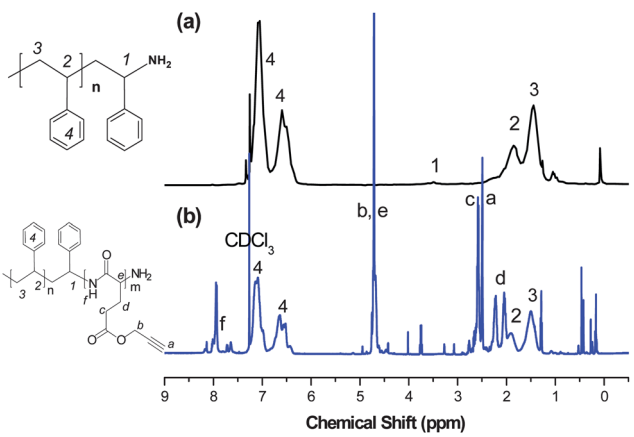

Fig. 3 ^{1}H NMR spectra of (a) PS–NH_2 and (b) PS-*b*-$PPLG_{10}$ (in $CDCl_3$ and 15 wt% TFA).

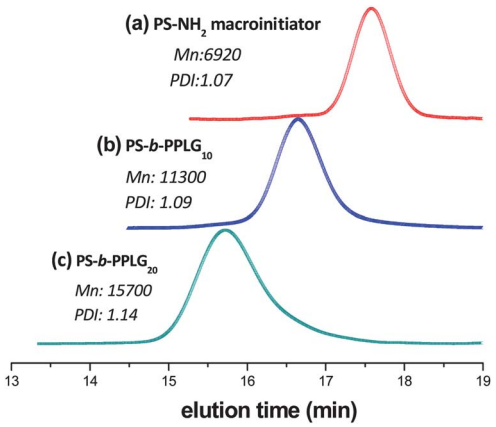

Fig. 4 GPC traces of (a) the PS–NH_2 macroinitiator, (b) PS-*b*-$PPLG_{10}$, and (c) PS-*b*-$PPLG_{20}$.

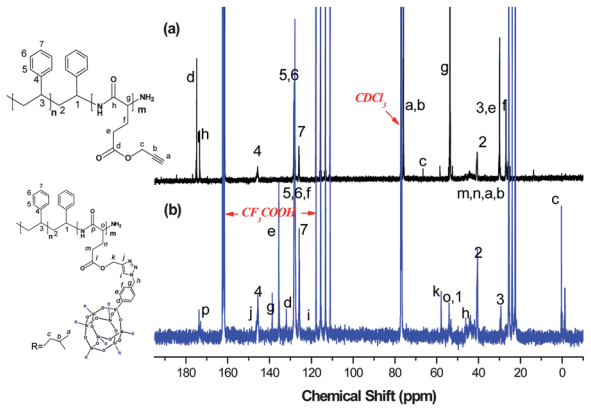

Fig. 6 ^{13}C NMR spectra of (a) PS-*b*-$PPLG_{10}$ and (b) PS-*b*-$PPLG_{10}$-*g*-POSS (in $CDCl_3$ and 15 wt% TFA).

molecular weights of the PS-*b*-PPLG copolymers used in this study, as determined through GPC and ^1H NMR spectroscopic analyses.

Synthesis of PS-*b*-(PPLG-*g*-POSS) by click reaction of PS-*b*-PPLG with N_3–POSS

Fig. 5 presents the ^1H NMR spectra of N_3–POSS, PS-*b*-PPLG, and PS-*b*-(PPLG-*g*-POSS). The signal at 4.36 ppm for the benzyl CH_2 group connected to the azide unit of N_3–POSS shifted downfield significantly (to 5.70 ppm) for PS-*b*-(PPLG-*g*-POSS). In addition, the signals for the isobutyl groups attached to the Si atoms of the POSS moiety appeared at approximately 0.63, 0.93, and 1.85 ppm. The proton on the nitrogen atom of PPLG resonated as a singlet at 7.9 ppm. The resonance at 8.2 ppm was due to the proton of the triazole structures formed through the click reactions, confirming the successful synthesis of PS-*b*-(PPLG-*g*-POSS). Fig. 6 presents the ^{13}C NMR spectra of PS-*b*-PPLG and PS-*b*-(PPLG-*g*-POSS); the C=O and amide carbon atom signals appeared in the ^{13}C NMR spectrum of PS-*b*-(PPLG-*g*-POSS) at 172.0 and 175.0 ppm, respectively, while those of the phenyl ring from N_3–POSS appeared at 128.1, 132.2, 135.4, and 140.0 ppm. The signals for the benzylic carbon atom (*C*-h), ester carbon atom (***C***-k), and amino acid α-carbon atom (NHCO*C*) appear at 50.0, 58.4, and 55.0 ppm (α-helical conformation),[44] respectively. The isobutyl carbon atoms of the POSS moiety were represented by signals at 0.2, 25.0, and 29.0 ppm. The signal of the alkyne carbon atoms of PPLG (originally at 73.4 ppm) disappeared, but two new peaks appeared at 125.1 and 144.0 ppm, representing the carbon atoms of the triazole structures resulting from the click reaction, confirming the successful synthesis of PS-*b*-(PPLG-*g*-POSS). The ^{29}Si NMR spectrum featured three sharp signals at −67.2, −67.9, and −81.8 ppm, corresponding to the Si atoms of the POSS molecules (Fig. 7). FTIR spectroscopic analysis also confirmed the complete disappearance of the characteristic signals for the azido and acetylene groups (Fig. 8). The signal at 2105 cm^{-1}, corresponding to the absorbance of the azido group of N_3–POSS, and the signal at 2130 cm^{-1}, corresponding to the acetylene group of PS-*b*-PPLG, were absent in the spectra of PS-*b*-(PPLG-*g*-POSS). The absorption bands of the SiOSi (siloxane) groups of the POSS moiety (at 1105 cm^{-1}) and the amide I groups of PS-*b*-PPLG (at 1657 cm^{-1}) appeared in the spectra of the PS-*b*-PPLG-*g*-POSS copolymers, indicating that the azido and acetylene functionalities had participated in the click reactions.

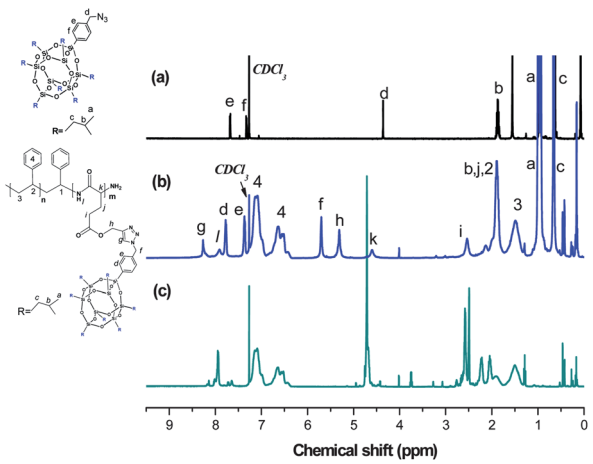

Fig. 5 ^1H NMR spectra of (a) N_3–POSS (in $CDCl_3$), (b) PS-*b*-$PPLG_{10}$-*g*-POSS and (c) PS-*b*-$PPLG_{10}$ (in $CDCl_3$ and 15 wt% TFA).

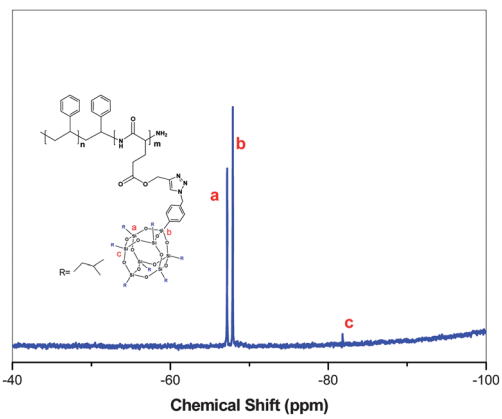

Fig. 7 ^{29}Si NMR spectrum of PS-*b*-$(PPLG\text{-}g\text{-}POSS)_{10}$.

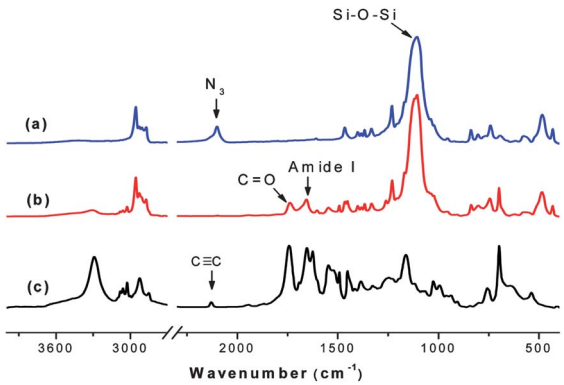

Fig. 8 FTIR spectra of (a) POSS–N_3, (b) PS-*b*-PPLG-*g*-POSS, and (c) PS-*b*-PPLG.

Thermal analyses of PS-*b*-(PPLG-*g*-POSS) copolymers

Fig. 9 presents DSC thermograms of the PS-*b*-PPLG and PS-*b*-(PPLG-*g*-POSS) copolymers. During the second heating run of each of the PS-*b*-PPLG copolymers, we observed (Fig. 9(b) and (c)) two glass transition temperatures (T_g, at *ca.* 90 and 20 °C) representing the PPLG (Fig. 9(d)) and PS (Fig. 9(a)) block segments, respectively; that is, phase separation occurred in the PS-*b*-PPLG copolymers. After grafting the POSS moiety onto PS-*b*-PPLG, we observed dramatic changes in the second-heating-run DSC trace. First, the glass transition temperature of the peptide segment in PS-*b*-(PPLG-*g*-POSS) increased significantly, to approximately 80 °C; the value of T_g for the peptide segment of PS-*b*-(PPLG-*g*-POSS) was higher (by *ca.* 50 °C) than that of the corresponding PS-*b*-PPLG copolymer. Second, an exothermic peak appeared near 120–140 °C and an endothermic peak near 175 °C, representing the crystallization and melting temperatures, respectively, of the isobutyl-POSS moieties.[63] The significant increase in the value of T_g of PS-*b*-(PPLG-*g*-POSS) was due to the nano-reinforcement effect, with the rigid cubic silsesquioxane cores of the POSS units on the PS-*b*-PPLG segments effectively restricting molecular chain motion.[63–66] In addition, specific interactions might occur between the POSS and PS-*b*-PPLG moieties in these graft polymers. The amide group of PS-*b*-PPLG might hydrogen bond with the siloxane group of POSS, thereby changing the secondary structure of PS-*b*-PPLG, possibly through the β-sheet conformation of PS-*b*-PPLG transforming into an α-helix rigid rod-like structure after incorporation of the POSS units in the PS-*b*-(PPLG-*g*-POSS) system. We used FTIR spectroscopy and WAXD analyses to characterize the transformation of the secondary structures of PS-*b*-PPLG and PS-*b*-(PPLG-*g*-POSS).

Using FTIR spectroscopy to study the conformation of the peptide segment

We recorded FTIR spectra at room temperature to obtain information relating to the conformation of the peptide segments in PS-*b*-PPLG and PS-*b*-PPLG-*g*-POSS (Fig. 10). First, we analyzed these spectra using the second derivative technique,[42] which indicated that the amide I band at 1655 cm^{-1} was characteristic of the α-helical secondary structure. For polypeptides possessing a β-sheet conformation, the position of the amide I band shifted to 1627 cm^{-1}, with a random coil or turn population located at 1693 cm^{-1}. The free C=O group of the side-chain group of PS-*b*-(PPLG-*g*-POSS) appeared at 1744 cm^{-1}; a peak at 1605 cm^{-1} corresponded to the benzene ring stretching of the side-chain groups of the POSS and PS segments (Fig. 10(b)). In the second step, we used the deconvolution technique with a series of Gaussian distributions using the Peakfit 4 program to quantify the fraction of each of the peaks [dashed line in Fig. 10]. Clearly, the fraction of α-helical secondary structures increased upon increasing the degree of polymerization (DP) of the PPLG block in PS-*b*-PPLG. This result is similar to that reported by Papadopoulos *et al.* for PBLG.[41] At low degrees of polymerization (DP; <18 for PBLG), both secondary structures are present; as the DP increases, however, the α-helical secondary structure is favored. In addition, all of the PS-*b*-(PPLG-*g*-POSS) copolymers obtained after performing the click reactions featured the α-helical secondary structure—even that with a relatively lower DP

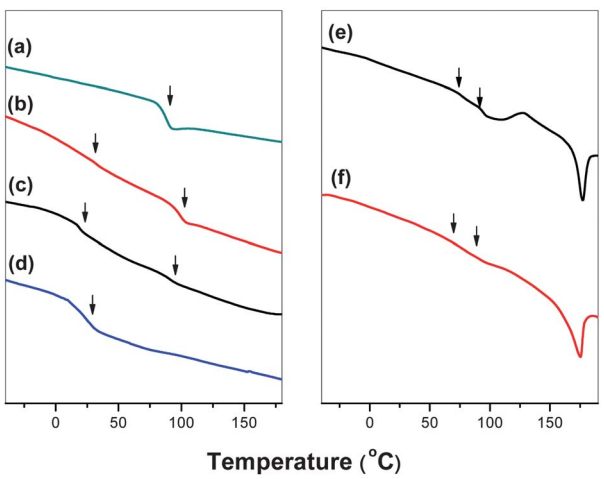

Fig. 9 DSC traces (second heating runs) of (a) PS–NH_2, (b) PS-*b*-$PPLG_{10}$, (c) PS-*b*-$PPLG_{20}$, (d) $PPLG_{20}$, (e) PS-*b*-$(PPLG\text{-}g\text{-}POSS)_{10}$, and (f) PS-*b*-$(PPLG\text{-}g\text{-}POSS)_{20}$.

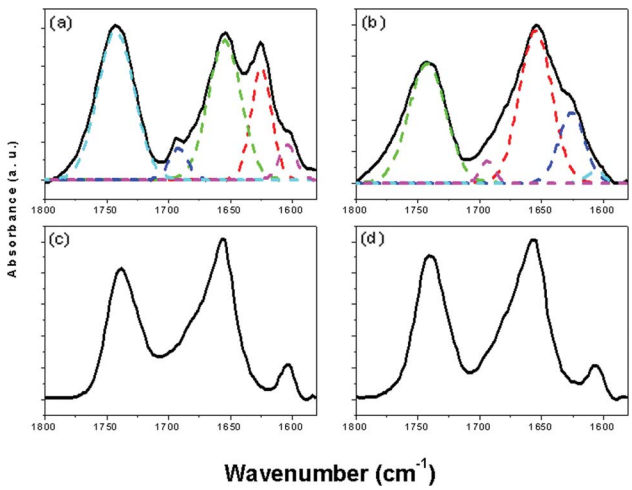

Fig. 10 FTIR spectra (recorded at room temperature) of (a) PS-*b*-$PPLG_{10}$, (b) PS-*b*-$PPLG_{20}$, (c) PS-*b*-$(PPLG\text{-}g\text{-}POSS)_{10}$ and (d) PS-*b*-$(PPLG\text{-}g\text{-}POSS)_{20}$.

[PS-*b*-(PPLG-*g*-POSS)$_{10}$]. We suspect that rigid POSS moieties in the side chain might enhance hydrogen bonding between the C=O groups and the amide linkages of the α-helical conformation.

We recorded temperature-dependent FTIR spectra to obtain information relating to the conformation of the peptide segment. Fig. 11 displays the spectra of PPLG$_{15}$, PS-*b*-PPLG$_{10}$, and PS-*b*-(PPLG-*g*-POSS)$_{10}$. The presence of amide I and amide II bands at 1655 and 1545 cm^{-1}, respectively, revealed the α-helical secondary structure of all samples. The amide I band shifted to 1626 cm^{-1} and the amide II band shifted to 1520 cm^{-1}, both corresponding to the β-sheet conformation at room temperature. Clearly, the secondary structure of the PPLG$_{15}$ oligomer was sensitive to changes in temperature, with β-sheets being more predominant at elevated temperatures, as revealed in Fig. 11(a), indicating the instability of the α-helical conformation at such a low DP. This finding is in agreement with previous observations: the oligopeptide almost exclusively adopts the β-sheet conformation at high temperature.[47] Fig. 11(b) displays the FTIR spectra of the PS-*b*-PPLG$_{10}$ diblock copolymer at various temperatures. Comparing these spectra with those of the PPLG$_{15}$ oligomer reveals significant stabilization of the α-helical conformation upon attachment of the PS segment, even though the DP of PPLG (10) in PS-*b*-PPLG$_{10}$ was lower than that of pure PPLG$_{15}$. Nevertheless, PS-*b*-PPLG$_{10}$ retained its β-sheet conformation at high temperature. Most interestingly, the FTIR spectra of PS-*b*-(PPLG-*g*-POSS)$_{10}$ at various temperatures revealed (Fig. 11(c)) that the α-helical secondary structure was significantly stabilized upon attachment of the rigid POSS structures, relative to the FTIR spectra of the PPLG homopeptide and the PS-*b*-PPLG diblock copolymer. Indeed, the α-helical secondary structure of PS-*b*-(PPLG-*g*-POSS)$_{10}$ remained almost unchanged upon increasing the temperature. Thus, the DP, the temperature, and the attachment of POSS are all factors strongly influencing the secondary structure.

We also used WAXD at 393 K to characterize the secondary structural changes of the PS-*b*-PPLG and PS-*b*-(PPLG-*g*-POSS) systems. The diffraction pattern of PS-*b*-PPLG$_{10}$ reveals (Fig. 12(a)) the presence of β-sheet secondary structures. The first peak at a value of q of 0.48 represents the distance ($d = 1.30$ nm) between the backbones of the antiparallel β-pleated sheet structure; the reflection at a value of q of 1.34 ($d = 4.68$ nm) represents the intermolecular distance between adjacent peptide chains within each lamella. Increasing the DP of the PPLG block in PS-*b*-PPLG$_{20}$ resulted in lowering of the intensity of the diffraction peak at a value of q of 0.48, associated with the β-sheet secondary structure, similar to the behavior in the FTIR spectra in Fig. 10. The three reflections at higher angles, with positions $1 : 3^{1/2} : 4^{1/2}$ relative to the primary peak (q^*), are indexed according to the (10), (11), and (20) reflections of a 2D hexagonal packing of cylinders composed of 18/5 α-helices with a cylinder distance of

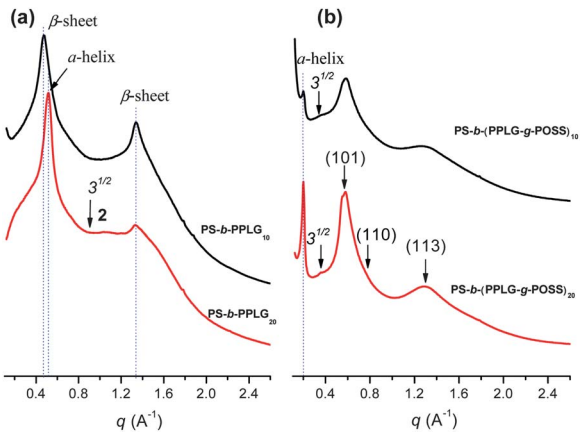

Fig. 12 WAXD patterns (recorded at 393 K) of (a) PS-*b*-PPLG and (b) PS-*b*-(PPLG-*g*-POSS) different DPs.

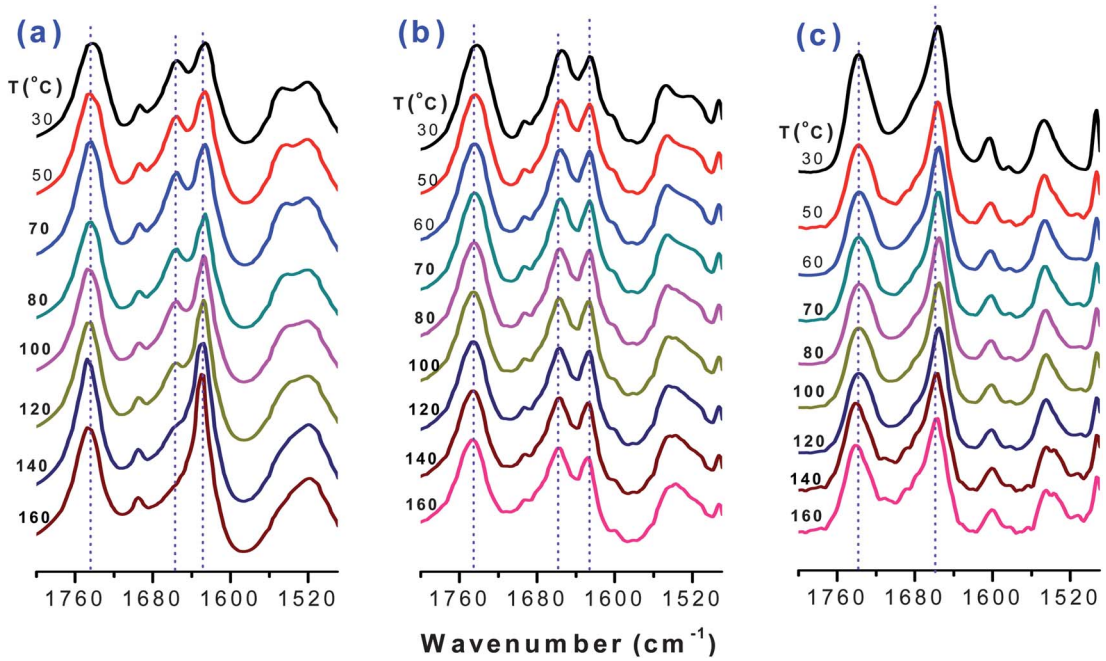

Fig. 11 Variable-temperature FTIR spectra of (a) PPLG$_{15}$, (b) PS-*b*-PPLG$_{10}$, and (c) PS-*b*-(PPLG-*g*-POSS)$_{10}$.

1.18 nm.[41] Additionally, the α-helical conformations were better packed in the longer peptide. From the FTIR spectra and WAXD data, we reached the following conclusion regarding the structures of PS-*b*-PPLG copolymers: at a low DP, β-sheet secondary structures are favored, but as the DP increases, the α-helical secondary structure is favored. The WAXD patterns of the PS-*b*-(PPLG-*g*-POSS) copolymers recorded at 393 K (Fig. 12(b)) differed dramatically from those of the PS-*b*-PPLG copolymers. For a considerable fraction of the peptide segments, we did not observe a sharp peak at a value of q of 1.34 for the β-sheet secondary structures of PS-*b*-(PPLG-*g*-POSS), unlike the situations for pure PPLG and PS-*b*-PPLG. Clearly, after the click reactions, the PS-*b*-(PPLG-*g*-POSS) copolymers with polypeptides featured a higher fraction of α-helical secondary structures than did the PS-*b*-PPLG copolymers, consistent with the FTIR spectroscopic data. Thus, the presence of POSS moieties on the PPLG side chains stabilized the PPLG α-helices, presumably through intramolecular hydrogen bonding. Thus, even if the unmodified peptide could adopt both α-helical and β-sheet conformations, the anchoring of POSS units to the side-chain polymer induced conformational stabilization, with most of the peptide segments becoming constrained in the α-helical secondary structure. We also observed the peak at a value of q of 0.58 accompanies two major diffraction angles and d-spacing distance, where (d_{hkl})-q = 0.58 (10.82 Å), q = 0.77 (8.15 Å), q = 1.34 (4.69 Å), that corresponded to the (hkl) diffraction planes (101), (110), and (113) for a hexagonal POSS crystal.[67] This finding is consistent with that from the DSC analyses, where endothermic peaks near 175 °C corresponded to the melting temperature of the POSS moiety. Structurally speaking, we would expect the incorporation of the rigid and bulky POSS moieties into the PPLG side chains to expand or swell the distance between the 2D hexagonally packed cylinders of α-helices of PPLG-*g*-POSS. Fig. 12(b) reveals that the WAXD pattern of the PS-*b*-(PPLG-*g*-POSS) copolymer features more than one strong additional diffraction angle (at q = 0.2) and a weak diffraction angle (at q = 0.35) relative to that of PS-*b*-PPLG. These two reflections with a relative position of 1 : $3^{1/2}$ correspond to 2D hexagonal packing of cylinders of PS-*b*-(PPLG-*g*-POSS) with an order spacing of approximately 31.4 Å. The PPLG blocks tether the POSS units on the side chain from its crystalline domains; meanwhile, the scattered POSS moieties gather and lock into the copolymers to form crystalline entities. To observe the correlation between the self-assembly of the hexagonally packed block polypeptides and the crystallization of the POSS units, we conducted SAXS analyses of the PS-*b*-$PPLG_{20}$ and PS-*b*-$(PPLG\text{-}g\text{-}POSS)_{20}$ systems at 393 K. In Fig. 13(a) and (b) we observe the short-range order of the cylindrical structures for both PS-*b*-$PPLG_{20}$ and PS-*b*-$(PPLG\text{-}g\text{-}POSS)_{20}$, with the maximum intensity appearing at values of q* of approximately 0.073 nm^{-1} (d = 8.53 nm) and 0.059 nm^{-1} (d = 10.51 nm), respectively, with the shoulder reflections appearing at $3^{1/2}q$*. From Flory theory,[68,69] the enthalpic contribution as well as chain stretching were caused by nanoparticle dispersion, which was also observed in PS-*b*-$(PPLG\text{-}g\text{-}POSS)_{20}$ (d = 10.51 nm) compared with PS-*b*-$PPLG_{20}$ (d = 8.53 nm). Clearly, the broad peak, assumed to be a Bragg reflection, at a value of q of 0.2 nm^{-1} corresponds to an ordered spacing of approximately

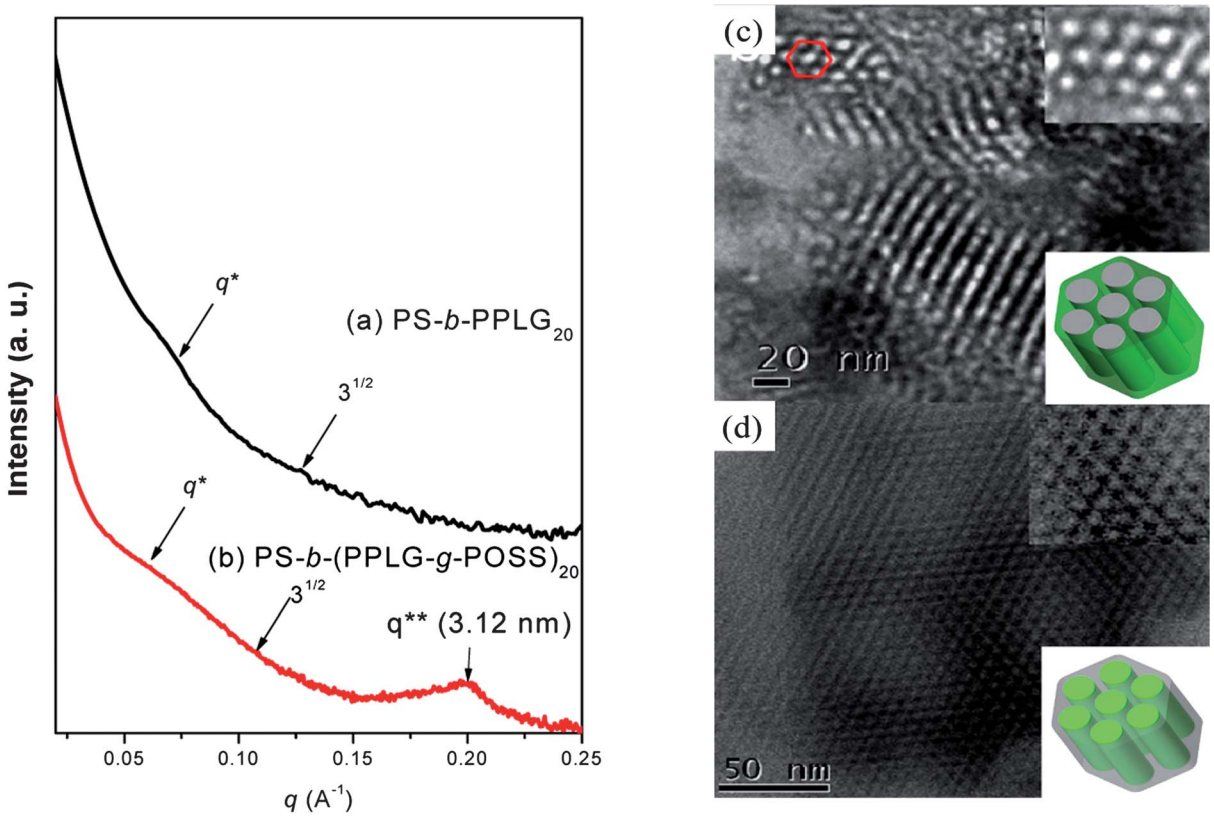

Fig. 13 (a and b) SAXS patterns (recorded at 393 K) and (c and d) TEM images of (a and c) PS-*b*-$PPLG_{20}$ and (b and d) PS-*b*-$(PPLG\text{-}g\text{-}POSS)_{20}$.

3.14 nm for PS-*b*-(PPLG-*g*-POSS)$_{20}$; this finding is consistent with the WAXD data. Fig. 13(c) and (d) present the corresponding TEM images of PS-*b*-PPLG$_{20}$ and PS-*b*-(PPLG-*g*-POSS)$_{20}$, respectively. After RuO_4 staining, the PS microdomains of PS-*b*-PPLG$_{20}$ appeared dark and the PPLG microdomains appeared light, indicating the short-range order of the cylinder structure. The inter-cylinder distance of the cylinder structures for PS-*b*-PPLG$_{20}$ was approximately 8 nm, consistent with the first peak in the SAXS analysis.[50] Fig. 13(d) displays the TEM image of PS-*b*-(PPLG-*g*-POSS)$_{20}$ without staining, revealing the presence of self-assembly cylinder structures with an inter-cylinder distance of approximately 10 nm. We attribute the dark regions to the POSS-rich layers, because the Si elements of POSS have a higher mass contrast than do the organic carbon or nitrogen functional groups of the PS and PPLG segments. Clearly, a phase inversion occurred from PS-*b*-PPLG to PS-*b*-(PPLG-*g*-POSS), due to the volume fraction of the PS segments (f_{PS}) in PS-*b*-PPLG changing significantly from 0.73 to 0.26 for PS-*b*-(PPLG-*g*-POSS), as calculated using the group contribution method.[70] Scheme 2(a) provides a schematic representation of the organization of the cylinders with α-helical conformations for PS-*b*-PPLG. The hexagonal periodicity with a value of *D* of 8.53 nm corresponds to the packing model of PS-*b*-PPLG$_{20}$; the diblock copolymer self-assembled hexagonally into long columns with the peptide segments oriented perpendicular to the director of the column. 2D hexagonal packing of cylinders with an inter-cylinder distance of 1.18 nm for PPLG (Scheme 2(a)), as calculated from the WAXD data. Scheme 2(b) provides a cartoon representation of the self-assembled structure formed from the PS-*b*-(PPLG-*g*-POSS) copolymer, where the average distance between the PS cylinders was 10.51 nm; the PPLG-*g*-POSS block segments formed 18/5 α-helices with a hexagonally packed cylinder distance of 3.14 nm, with POSS aggregation driving the packing into a hexagonal packing lattice. Hierarchical self-assembly structures were found in this PS-*b*-(PPLG-*g*-POSS) copolymers including microphase separation inducing self-assembly hexagonal cylinder structure between PS and PPLG-*g*-POSS diblock copolymer segments (d = 10.51 nm), the hexagonal packing cylinder distance of α-helices from PPLG-*g*-POSS segment (d = 3.14 nm) that is oriented perpendicularly to the direction of the cylinder structure from diblock copolymer segments, and the POSS aggregation drives to pack into the hexagonal lattice that is oriented parallel to the director of the cylinder structure from diblock copolymer segments, but perpendicularly to the director cylinder of α-helices from PPLG-*g*-POSS segment as shown in Scheme 2(b).

Conclusions

We have used a combination of ATRP, ROP, and click chemistry to prepare novel hierarchically self-assembling PS-*b*-(PPLG-*g*-POSS) block copolymers. After attaching POSS nanoparticles to the side chains of PS-*b*-PPLG copolymers, the fraction of α-helical secondary structures increased and exhibited greater conformation stability and superior thermal properties, including T_g behavior, relative to those of the unmodified PS-*b*-PPLG copolymers. WAXD, SAXS, and TEM analyses confirmed that the PS-(*b*-PPLG-*g*-POSS) copolymers underwent hierarchical self-assembly to form hexagonally packed cylindrical nanostructures, featuring α-helical conformations and POSS aggregates. This new organic/inorganic hybrid block copolymer, containing polypeptide and POSS segments, would have the potential application of the biological and integrated circuit materials.

Acknowledgements

This study was supported financially by the National Science Council, Taiwan, Republic of China, under contracts NSC 100-2221-E-110-029-MY3 and NSC 100-2628-E-110-001.

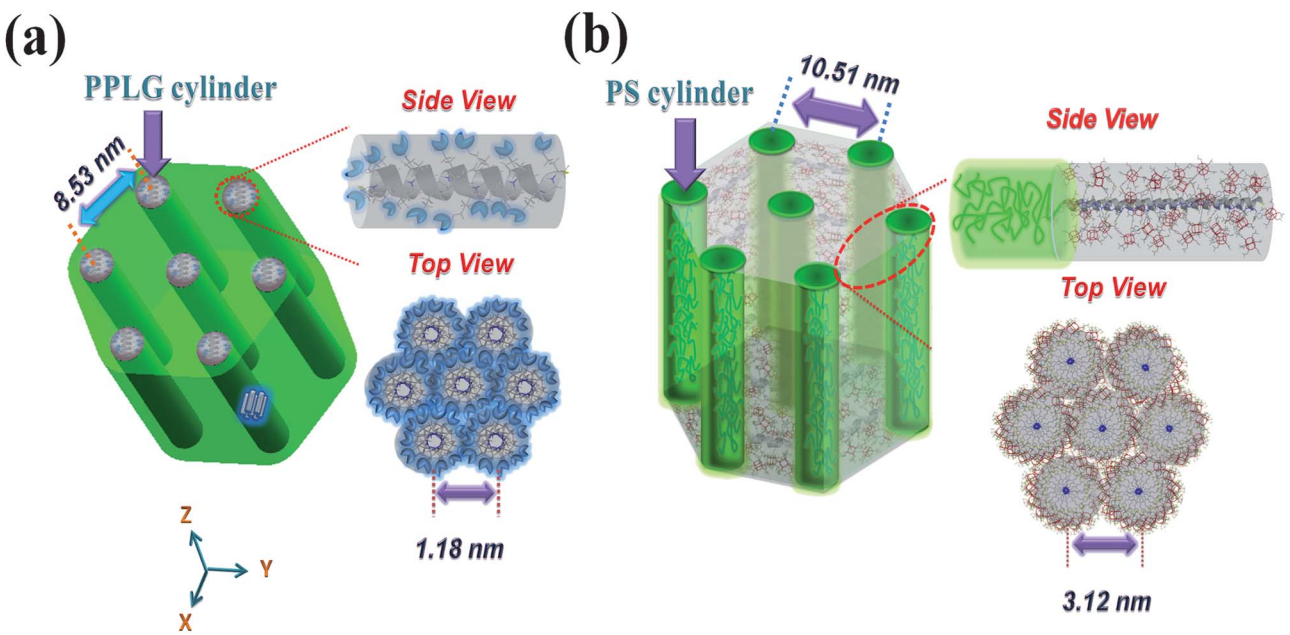

Scheme 2 Hierarchical self-assembled structures formed from (a) PS-*b*-PPLG and (b) PS-*b*-(PPLG-*g*-POSS) diblock.

Notes and references

1 J. Y. Cheng, A. M. Mayes and C. A. Ross, *Nat. Mater.*, 2004, **3**, 823–828.
2 C. J. Hawker and T. P. Russell, *MRS Bull.*, 2005, **30**, 952–966.
3 J. Y. Cheng, C. A. Ross, H. I. Smith and E. L. Thomas, *Adv. Mater.*, 2006, **18**, 2505–2521.
4 S. C. Chen, S. W. Kuo and F. C. Chang, *Langmuir*, 2011, **27**, 10197–10205.
5 H. W. Shen, L. F. Zhang and A. Eisenberg, *J. Am. Chem. Soc.*, 1999, **121**, 2728–2740.
6 J. Ruokolainen, M. Saariaho, O. Ikkala, G. ten Brinke, E. L. Thomas, M. Torkkeli and R. Serimaa, *Macromolecules*, 1999, **32**, 1152–1158.
7 S. W. Kuo, P. H. Tung, C. L. Lai, K. U. Jeong and F. C. Chang, *Macromol. Rapid Commun.*, 2008, **29**, 229–233.
8 S. C. Chen, S. W. Kuo, U. S. Jeng and F. C. Chang, *Macromolecules*, 2010, **43**, 1083–1092.
9 C. H. Lu, F. C. Chang and S. W. Kuo, *Macromol. Chem. Phys.*, 2010, **211**, 1339–1347.
10 R. M. Ho, Y. W. Chiang, S. C. Lin and C. K. Chen, *Prog. Polym. Sci.*, 2011, **36**, 376–453.
11 R. M. Ho, C. K. Chen and Y. W. Chiang, *Macromol. Rapid Commun.*, 2009, **30**, 1439.
12 S. G. Yang, X. F. Yu, L. Wang, Y. F. Tu, J. X. Zheng, J. T. Xu, R. M. Van Horn and S. Z. D. Cheng, *Macromolecules*, 2010, **43**, 3018–3026.
13 L. Zhu, P. Huang, W. Y. Chen, Q. Ge, R. P. Quirk, S. Z. D. Cheng, E. L. Thomas, B. Lotz, B. S. Hsiao, F. J. Yeh and L. Z. Liu, *Macromolecules*, 2002, **35**, 3553–3562.
14 P. Bhargava, J. X. Zheng, P. Li, R. P. Quirk, F. W. Harris and S. Z. D. Cheng, *Macromolecules*, 2006, **39**, 4880–4888.
15 V. S. D. Veot, T. E. Pick, S. M. Park, M. Moritz, A. T. Hammack, J. J. Urban, D. F. Ogletree, D. L. Olynick and B. A. Helms, *J. Am. Chem. Soc.*, 2011, **133**, 2812–2815.
16 J. G. Son, A. F. Hannon, K. W. Gotrik, A. Alexander-Katz and C. A. Ross, *Adv. Mater.*, 2011, **23**, 634–639.
17 M. Ramanathan, S. B. Darling and D. C. Mancini, *Adv. Sci. Lett.*, 2011, **4**, 437–441.
18 Y. Z. Ni, R. Rulkens and I. Manners, *J. Am. Chem. Soc.*, 1996, **118**, 4102–4114.
19 S. W. Kuo and F. C. Chang, *Prog. Polym. Sci.*, 2011, **36**, 1649–1696.
20 S. H. Phillips, T. S. Haddad and S. J. Tomczak, *Curr. Opin. Solid State Mater. Sci.*, 2004, **8**, 21–29.
21 J. E. Mark, *Acc. Chem. Res.*, 2004, **37**, 946–953.
22 K. Pielichowaski, J. Niuguna, B. Janowski and J. Pielichowski, *Adv. Polym. Sci.*, 2006, **201**, 225–296.
23 P. D. Lickiss and F. Rataboul, *Adv. Organomet. Chem.*, 2008, **57**, 1–116.
24 H. Xu, S. W. Kuo, J. S. Lee and F. C. Chang, *Macromolecules*, 2002, **35**, 8788–8793.
25 S. W. Kuo, H. F. Lee, W. J. Huang, K. U. Jeong and F. C. Chang, *Macromolecules*, 2009, **42**, 1619–1626.
26 S. W. Kuo, Y. C. Wu, C. H. Lu and F. C. Chang, *J. Polym. Sci., Part B: Polym. Phys.*, 2009, **47**, 811–819.
27 C. F. Huang, S. W. Kuo, F. J. Lin, W. J. Huang, C. F. Wang, W. Y. Chen and F. C. Chang, *Macromolecules*, 2006, **39**, 300–308.
28 C. C. Cheng, C. H. Chien, Y. C. Yen, Y. S. Ye, F. H. Ko, C. H. Lin and F. C. Chang, *Acta Mater.*, 2009, **57**, 1938–1946.
29 H. M. Lin, S. Y. Wu, P. Y. Huang, C. F. Huang, S. W. Kuo and F. C. Chang, *Macromol. Rapid Commun.*, 2006, **27**, 1550–1555.
30 B. H. Yang, H. Y. Xu, Z. Z. Yang and X. Y. Liu, *J. Mater. Chem.*, 2009, **19**, 9038–9044.
31 Y. L. Liu and M. H. Fangchiang, *J. Mater. Chem.*, 2009, **19**, 3643–3647.
32 C. H. Lu, F. C. Chang and S. W. Kuo, *Macromol. Chem. Phys.*, 2010, **211**, 1339–1347.
33 J. Pyun and K. Matyjaszewski, *Macromolecules*, 2000, **33**, 217–220.
34 J. Pyun, K. Matyjaszewski, J. Wub, G. M. Kimb, S. B. Chunb, T. Patrick and A. Mather, *Polymer*, 2003, **44**, 2739–2750.
35 B. X. Fu, A. Lee and T. S. Haddad, *Macromolecules*, 2004, **37**, 5211–5218.
36 D. B. Drazkowski, A. Lee, T. S. Haddad and D. J. Cookson, *Macromolecules*, 2006, **39**, 1854–1863.
37 D. B. Drazkowski, A. Lee and T. S. Haddad, *Macromolecules*, 2007, **40**, 2798–2805.
38 T. Hirai, M. Leolukman, T. Hayakawa, M. A. Kamimoto and P. Gopalan, *Macromolecules*, 2008, **41**, 4558–4570.
39 T. Hirai, M. Leolukman, S. Jin, R. Goseki, Y. Ishida, M. A. Kakimoto, T. Hayakawa, M. Ree and P. Gopalan, *Macromolecules*, 2009, **42**, 8835–8843.
40 T. Hirai, M. Leolukman, C. C. Liu, E. Han, Y. J. Kim, Y. Ishida, T. Hayakawa, M. A. Kakimoto, P. F. Nealey and P. Gopalan, *Adv. Mater.*, 2009, **21**, 4334–4338.
41 P. Papadopoulos, G. Floudas, H. A. Klok, I. Schnell and T. Pakula, *Biomacromolecules*, 2004, **5**, 81–91.
42 A. Sanchez-Ferrer and R. Mezzenga, *Macromolecules*, 2010, **43**, 1093–1100.
43 Q. H. Zhou, J. K. Zheng, Z. H. Shen, X. H. Fan, X. F. Chen and Q. F. Zhou, *Macromolecules*, 2010, **43**, 5637–5646.
44 H. F. Lee, H. S. Sheu, U. S. Jeng, C. F. Huang and F. C. Chang, *Macromolecules*, 2005, **38**, 6551–6558.
45 P. Papadopoulos, G. Floudas, I. Schnell, T. Aliferis, H. Iatrou and N. Hadjichristidis, *Biomacromolecules*, 2005, **6**, 2352–2361.
46 H. A. Klok, J. F. Langenwalter and S. Lecommandoux, *Macromolecules*, 2000, **33**, 7819–7826.
47 S. Lecommandoux, M. F. Achard, J. F. Langenwalter and H. A. Klok, *Macromolecules*, 2001, **34**, 9100–9111.
48 J. S. Crespo, S. Lecommandoux, R. Borsali, H. A. Klok and V. Soldi, *Macromolecules*, 2003, **36**, 1253–1256.
49 P. Papadopoulos, G. Floudas, I. Schnell, I. Lieberwirth, T. Q. Nguyen and H. A. Klok, *Biomacromolecules*, 2006, **7**, 618–626.
50 H. A. Klok and S. Lecommandoux, *Adv. Polym. Sci.*, 2006, **202**, 75–111.
51 G. Floudas, P. Papadopoulos, H. A. Klok, G. W. M. Vandermeulen and J. Rodriguez-Hernandez, *Macromolecules*, 2003, **36**, 3673–3683.
52 I. K. Kang, Y. Ito, M. Sisido and Y. Imanishi, *Biomaterials*, 1988, **9**, 349–355.
53 C. Hua, C. M. Dong and Y. Wei, *Biomacromolecules*, 2009, **10**, 1140–1148.
54 C. J. Huang and F. C. Chang, *Macromolecules*, 2008, **41**, 7041–7052.
55 B. Perly, A. Douy and B. Gallot, *Makromol. Chem.*, 1976, **177**, 2569–2589.
56 A. Nakajima, T. Hayashi, K. Kugo and K. Shinoda, *Macromolecules*, 1979, **12**, 840–843.
57 S. W. Kuo, H. F. Lee and F. C. Chang, *J. Polym. Sci., Part A: Polym. Chem.*, 2008, **46**, 3108–3119.
58 X. Kong and S. A. Jenekhe, *Macromolecules*, 2004, **37**, 8180–8183.
59 Y. C. Lin and S. W. Kuo, *J. Polym. Sci., Part A: Polym. Chem.*, 2011, **49**, 2127–2137.
60 A. C. Engler, H. Lee and P. T. Hammond, *Angew. Chem., Int. Ed.*, 2009, **48**, 9334–9338.
61 C. Xiao, C. Zhao, P. He, Z. Tang, X. Chen and X. Jing, *Macromol. Rapid Commun.*, 2010, **31**, 991–997.
62 Y. C. Lin and S. W. Kuo, *Polym. Chem.*, 2012, **3**, 162–171.
63 W. B. Zhang, Y. Li, X. Li, X. Dong, X. Yu, C. L. Wang, C. Wesdemiotis, R. P. Quirk and S. Z. D. Cheng, *Macromolecules*, 2011, **44**, 2589–2596.
64 Y. Ishida, T. Hira, R. Goseki, M. Tokita, M. A. Kakimoto and T. Hayakawa, *J. Polym. Sci., Part A: Polym. Chem.*, 2011, **49**, 2653–2664.
65 Y. C. Wu and S. W. Kuo, *Polymer*, 2010, **51**, 3948–3955.
66 K. W. Huang and S. W. Kuo, *Macromol. Chem. Phys.*, 2010, **211**, 2301–2311.
67 C. H. Lu, S. W. Kuo, C. F. Huang and C. F. Chang, *J. Phys. Chem. C*, 2009, **113**, 3517–3524.
68 A. C. Balazs, T. Emrick and T. P. Russell, *Science*, 2006, **314**, 1107–1110.
69 M. E. Mackay, A. Tuteja, P. M. Duxbury, C. J. Hawker, B. V. Horn, Z. Guan, G. Chen and R. S. Krishna, *Science*, 2006, **311**, 1740–1743.
70 M. M. Coleman and P. C. Painter, *Miscible Polymer Blend-Background and Guide for Calculations and Design*, DEStech Publications Inc., 2006.